Supporting information for: Ion Transport and the True Transference Number in Nonaqueous Polyelectrolyte Solutions for Lithium-Ion Batteries

Kara D. Fong,[†,‡] Julian Self,[¶,‡] Kyle M. Diederichsen,[†,‡] Brandon M. Wood,[§,‡] Bryan D. McCloskey,[*,†,‡] and Kristin A. Persson[*,¶,‡]

†*Department of Chemical and Biomolecular Engineering, University of California, Berkeley*

‡*Energy Technologies Area, Lawrence Berkeley National Laboratory*

¶*Department of Materials Science and Engineering, University of California, Berkeley*

§*Department of Applied Science and Technology, University of California, Berkeley*

E-mail: bmcclosk@berkeley.edu; kapersson@lbl.gov

Additional Methods

Ion Speciation

Free lithium ions, solvent-separated ion pairs (SSIPs), and contact ion pairs (CIPs) or larger aggregates (AGG) were identified from the cation-anion (Li^+-S (SO_3^-)) radial distribution functions (RDFs), plotted for each concentration in Figure S1. A lithium ion is considered part of a CIP or AGG if there is at least one sulfonate anion, specifically the sulfur atom, within the cutoff distance defined by the minimum after the first peak in the Li^+-S (SO_3^-) RDF (4.5 Å for all concentrations). SSIPs were defined analogously using the minimum after

the second RDF peak (9.5-9.7 Å), and free lithium ions were those without any anions within the SSIP or CIP cutoff distances. Analysis of larger aggregate structures was undertaken with the aid of the Python package NetworkX,[S1] and visualizations of the most common Li^+ solvation environments were generated using the software Cytoscape.[S2]

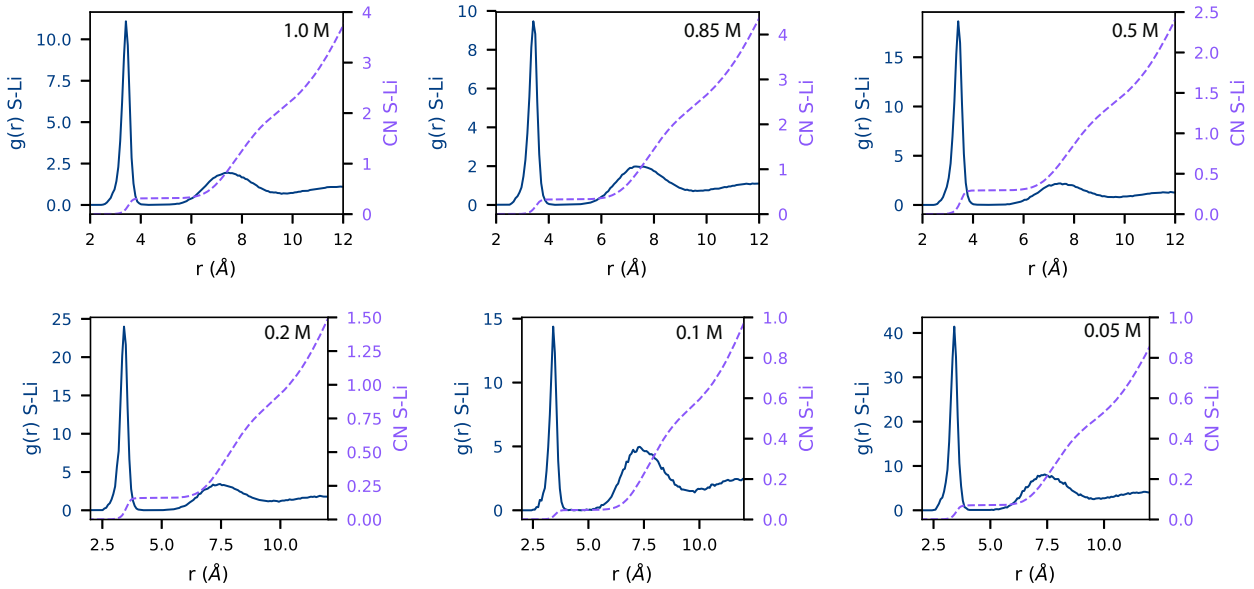

Figure S1: Lithium-sulfur (SO_3^-) radial distribution functions (left axis) and coordination numbers (right axis) at each concentration studied.

Polymer Conformation

Polyelectrolyte chain size was characterized using both the end-to-end distance as well as the radius of gyration, the latter of which is determined using:[S3]

$$R_g^2 = \frac{1}{M}\left\langle \sum_{i=1}^{n} m_i \left| \boldsymbol{r}_i - \boldsymbol{r}_{poly,cm} \right|^2 \right\rangle \tag{1}$$

where n is the total number of atoms in the chain, M is the total mass of the polymer, m_i is the mass of atom i, $\boldsymbol{r}_i$ is the position vector of atom i, and $\boldsymbol{r}_{poly,cm}$ is the position vector of the polymer center of mass.

While a number of models exist to calculate the persistence length L_p of a polyelectrolyte

chain,[S4,S5] the data presented in this work are calculated based on the orientational correlation function $G(l)$, which characterizes the orientational memory along the chain backbone:[S6]

$$G(l) = \frac{1}{N_b - l} \sum_{s=0}^{N_b - l - 1} \left\langle \boldsymbol{n}_s \cdot \boldsymbol{n}_{s+l} \right\rangle \tag{2}$$

Here $\boldsymbol{n}_s$ is the unit vector originating at backbone atom s and pointing along the polymer backbone, N_b is the total number of bonds in the polymer backbone, and l is the number of bonds separating unit vectors $\boldsymbol{n}_s$ and $\boldsymbol{n}_{s+l}$. The angular brackets denote an average of all chain conformations over time. To convert this orientational correlation function into a persistence length, it has been recently suggested that $G(l)$ should be fit to a biexponential function,[S6–S8]

$$G(l) = (a)exp\left(- \frac{|l|}{L_p} \right) + (1 - a)exp\left(- \frac{|l|}{L_{short}} \right) \tag{3}$$

which is in good qualitative agreement with our calculated $G(l)$ functions. The first exponential decay constant, L_p, is the total persistence length of the chain, which is the sum of the intrinsic persistence length of the uncharged chain as well as the electrostatic persistence length. It is this L_p value which is the subject of our analysis in this work. The decay constant of the second exponential, L_{short}, describes additional orientational correlations present at short length scales, and a is an additional fitting parameter.[S9]

Diffusion Coefficients

Diffusion coefficients of lithium ions and the polyelectrolyte center of mass were calculated based on the mean-square displacement (MSD, $\langle \Delta r(t)^2 \rangle$),

$$\langle \Delta r(t)^2 \rangle = \frac{1}{N} \left\langle \sum_{i=1}^{N} \left| \boldsymbol{r}_i(t) - \boldsymbol{r}_i(0) - [\boldsymbol{r}_{cm}(t) - \boldsymbol{r}_{cm}(0)] \right|^2 \right\rangle \tag{4}$$

where N is the total number of atoms/molecules, $\boldsymbol{r}_i(t)$ is the position vector of species i at time t, and $\boldsymbol{r}_{cm}$ is the position of the center of mass of the entire system, which we include

to correct for any drift in the center of mass of the simulation box. The angular brackets indicate the average over all time origins within the trajectory. From the MSD, the Einstein relation can be used to compute the self-diffusion coefficient D:

$$D = \frac{1}{6} \lim_{t \to \infty} \frac{d}{dt} \langle \Delta r(t)^2 \rangle \tag{5}$$

For an equilibrated system at sufficiently long simulation times, the system should be in the diffusive regime such that the MSD curve is linear with respect to time. That is, $\langle \Delta r(t)^2 \rangle \propto t^{\beta}$, with $\beta = 1$. We ensure that all simulations in this work are run sufficiently long to achieve this linear behavior: we calculate average β values of 0.97 for Li^+ (ranging from 0.95 to 1.01) and 0.98 for the polyion center of mass (ranging from 0.87 to 1.06). Note that the statistics for the polymer are slightly inferior to that of the lithium ion: for Li^+ we average over all 43 ions in the system, which cannot be done for our single polymer chain. Nevertheless, our ranges of β are commonly accepted to be sufficiently linear for diffusion coefficient analysis.[S10] Figure S2a demonstrates this linear behavior for both the lithium ions and polymer for a representative simulation.

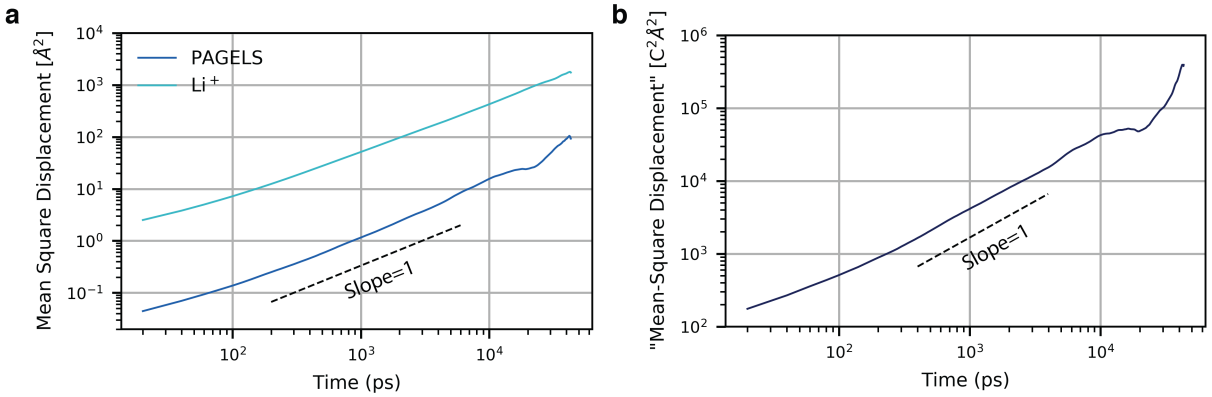

Figure S2: Representative examples of the linear behavior required to calculate (a) diffusion coefficients and (b) ionic conductivity. A slope of one (corresponding to linear data on a log-log plot) is indicated on each plot. The effective "mean square displacement" on the y-axis of panel (b) is the quantity in angular brackets in Eq. (6) of the SI. Data for these plots was for the system at a concentration of 0.85 M.

Note that data for our trajectory analysis has been collected every 20 ps. As a result, any

non-Fickian diffusive processes present at very short times are not clearly shown in the MSD curve of Figure S2a. As noted in previous MD simulations of polyelectrolytes, at short times we expect to see a ballistic regime with a log-log slope of 2, followed by a sub-diffusive regime with a slope less than one before finally reaching the Fickian regime with a log-log slope of one.[S11] To demonstrate that we do indeed observe these phenomena, we have performed a simulation collecting data every 10 fs and plotted the polymer center of mass MSD data in Figure S3.

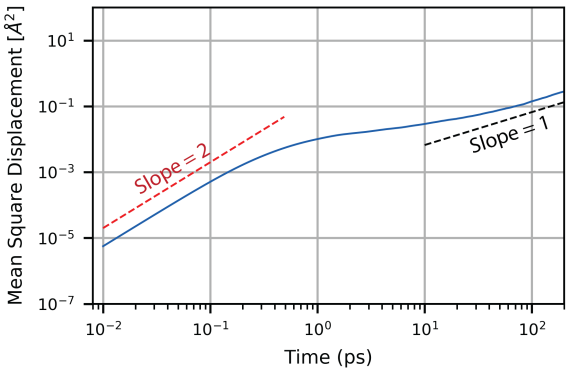

Figure S3: Short-time behavior of the polymer center of mass mean-square displacement for the system at a concentration of 0.85 M.

Ionic Conductivity

Ionic conductivity σ can be calculated from the following relation:

$$\sigma = \frac{1}{6k_BTV} \lim_{t\to\infty} \frac{d}{dt} \left\langle \sum_i \sum_j q_i q_j [\boldsymbol{r}_i(t) - \boldsymbol{r}_i(0)] \cdot [\boldsymbol{r}_j(t) - \boldsymbol{r}_j(0)] \right\rangle \tag{6}$$

where q_i is the charge of species i, k_BT is the thermal energy, and V is volume. This Einstein relation is derived from the Green-Kubo equation relating ionic conductivity with the microscopic charge current.[S12,S13]

As is the case with diffusion coefficient calculations, a mathematically rigorous analysis of the conductivity requires the term enclosed in the angular brackets of Eq. (6) to be linear

in time. The simulations performed here all reached the linear regime, with β values (defined as the extent of linearity analogously to the diffusion coefficient analysis above) between 0.84 and 1.04 for all concentrations. Results from a representative simulation are shown in Figure S2b.

The ionic conductivity can be decomposed into separate terms, each corresponding to a different type of uncorrelated or correlated ion motion, namely the cation-self (σ^s_{cat}), anion-self (σ^s_{an}), cation-distinct (σ^d_{cat}), anion-distinct(σ^d_{an}), and cation-anion-distinct ($\sigma^d_{cat,an}$) conductivities.

$$\sigma = \sigma^s_{cat} + \sigma^s_{an} + \sigma^d_{cat} + \sigma^d_{an} + 2\sigma^d_{cat,an} \tag{7}$$

These various conductivity contributions are defined as:

$$\sigma^s_{cat} = \frac{1}{6k_BTV} \lim_{t\to\infty} \frac{d}{dt} \left\langle \sum_{i_{cat}} q^2_{i_{cat}} [\boldsymbol{r}_{i_{cat}}(t) - \boldsymbol{r}_{i_{cat}}(0)] \cdot [\boldsymbol{r}_{i_{cat}}(t) - \boldsymbol{r}_{i_{cat}}(0)] \right\rangle \tag{8}$$

$$\sigma^s_{an} = \frac{1}{6k_BTV} \lim_{t\to\infty} \frac{d}{dt} \left\langle \sum_{i_{an}} q^2_{i_{an}} [\boldsymbol{r}_{i_{an}}(t) - \boldsymbol{r}_{i_{an}}(0)] \cdot [\boldsymbol{r}_{i_{an}}(t) - \boldsymbol{r}_{i_{an}}(0)] \right\rangle \tag{9}$$

$$\sigma^d_{cat} = \frac{1}{6k_BTV} \lim_{t\to\infty} \frac{d}{dt} \left\langle \sum_{i_{cat}} \sum_{j_{cat}\neq i_{cat}} q_{i_{cat}} q_{j_{cat}} [\boldsymbol{r}_{i_{cat}}(t) - \boldsymbol{r}_{i_{cat}}(0)] \cdot [\boldsymbol{r}_{j_{cat}}(t) - \boldsymbol{r}_{j_{cat}}(0)] \right\rangle \tag{10}$$

$$\sigma^d_{an} = \frac{1}{6k_BTV} \lim_{t\to\infty} \frac{d}{dt} \left\langle \sum_{i_{an}} \sum_{j_{an}\neq i_{an}} q_{i_{an}} q_{j_{an}} [\boldsymbol{r}_{i_{an}}(t) - \boldsymbol{r}_{i_{an}}(0)] \cdot [\boldsymbol{r}_{j_{an}}(t) - \boldsymbol{r}_{j_{an}}(0)] \right\rangle \tag{11}$$

$$\sigma^d_{cat,an} = \frac{1}{6k_BTV} \lim_{t\to\infty} \frac{d}{dt} \left\langle \sum_{i_{cat}} \sum_{j_{an}} q_{i_{cat}} q_{j_{an}} [\boldsymbol{r}_{i_{cat}}(t) - \boldsymbol{r}_{i_{cat}}(0)] \cdot [\boldsymbol{r}_{j_{an}}(t) - \boldsymbol{r}_{j_{an}}(0)] \right\rangle \tag{12}$$

Due to challenges in reaching the linear regime for some of these self- and distinct-conductivity terms, the derivatives in Eq. (8) - Eq. (12) were approximated by finite difference at $t = 2$ ns and $t = 0$ ns. Note that averaging is performed over all time origins in the trajectory (as denoted by the angular brackets in these equations). Hence the analysis averages the system behavior for all time differences of 2 ns within the entire 40 ns simulation. It was ensured that the choice of upper time bound in the finite difference calculation did not appreciably

affect any trends as a function of concentration.

Diffusion Mechanism

The diffusion mechanism of species i relative to species j (i.e. structure-diffusion versus vehicular motion) was evaluated by calculating the lifetime correlation function, $P_{ij}(t)$:[S14,S15]

$$P_{ij}(t) = \left\langle H_{ij}(t) H_{ij}(0) \right\rangle \tag{13}$$

Here $H_{ij}(t)$ is one if i and j are neighbors at time t and zero otherwise. Two species are considered neighbors if they are within a given cutoff distance. In this work, we calculate $P_{ij}(t)$ for three species pairs: Li^+-O (DMSO), Li^+- S (SO_3^-), and S (SO_3^-)-O (DMSO). The cutoff distance for these pairs was defined as the minimum after the first peak of the RDF to capture the first coordination shell. Additionally, the lifetime correlation function of lithium relative to sulfonate anions in the second coordination shell (i.e. solvent-separated ion pairs) was calculated by deeming two ions neighbors if the distance between them is between the first and second minima of the Li^+-S (SO_3^-) RDF.

The lifetime correlation function P_{ij} is subsequently converted into a residence time τ_{ij} of i and j neighbor pairs via a biexponential fit:[S16]

$$P_{ij}(t) = \alpha exp\left(\frac{-t}{\tau_{ij}}\right)^{\delta} + (1-\alpha) exp\left(\frac{-t}{\tau_{ij,short}}\right) \tag{14}$$

where τ_{ij}, $\tau_{ij,short}$, α, and δ are fitting parameters. The first term in this expression gives the relevant residence time for inferring diffusion mechanisms, while the second term can be attributed to sub-diffusive processes at shorter timescales. The parameter δ varies between 0 and 1, with deviations from unity corresponding to the presence of multiple modes of diffusion with different timescales.[S17] Here we observe $\delta > 0.99$ for all pairs of species, with the exception of Li^+- S (SO_3^-) (CIP), where δ varied between 0.8 and 1.

Finally, this residence time is expressed as a characteristic diffusion length L_{ij} by incor-

porating the diffusion coefficient of the solvent:

$$L_{ij} = \sqrt{6 D_{solvent} \tau_{ij}} \tag{15}$$

This conversion corrects for the effect of changing overall solution viscosity across concentrations, enabling accurate comparison of diffusion mechanisms.

Statistical Error Analysis

Statistical error values were obtained through a combination of independent simulation replicates and time averaging of individual simulations. Note that these are statistical errors due to the inherently limited sampling of an MD simulation, not errors arising from the model itself such as the choice of force field parameters.

The majority of the error data reported herein are obtained through block averaging.[S13,S18,S19] For a given dynamical quantity, such as the fraction of free Li^+ ions or the polymer radius of gyration, we can calculate the statistical uncertainty of the average value by computing the variance of multiple statistically independent observations of the quantity. Simply evaluating the variance of the data at every snapshot of the trajectory will underestimate the true error due to the inherent correlations within the system. Thus, to calculate the true statistical error, we must split the simulations into uncorrelated blocks, then compute the mean value of our quantity of interest for each block. Our final estimate of the uncertainty is then the standard deviation of these blocked averages (including both those from the same simulation as well as those from the independent duplicate run). The block length which yields uncorrelated data is not known a priori, so the error is plotted over a range of block lengths, as in Figure S4. When the error becomes independent of block length, a suitable block length has been reached such that each block is uncorrelated from the rest.

Block averaging could not be performed for some quantities of interest (the self- and

distinct-conductivities as well as the ion aggregate size distributions) due to poor statistics; proper fits to the data could only be obtained using the full 40 ns trajectory. For these quantities, the reported error bars are the standard deviation of the two independent 40 ns duplicates.

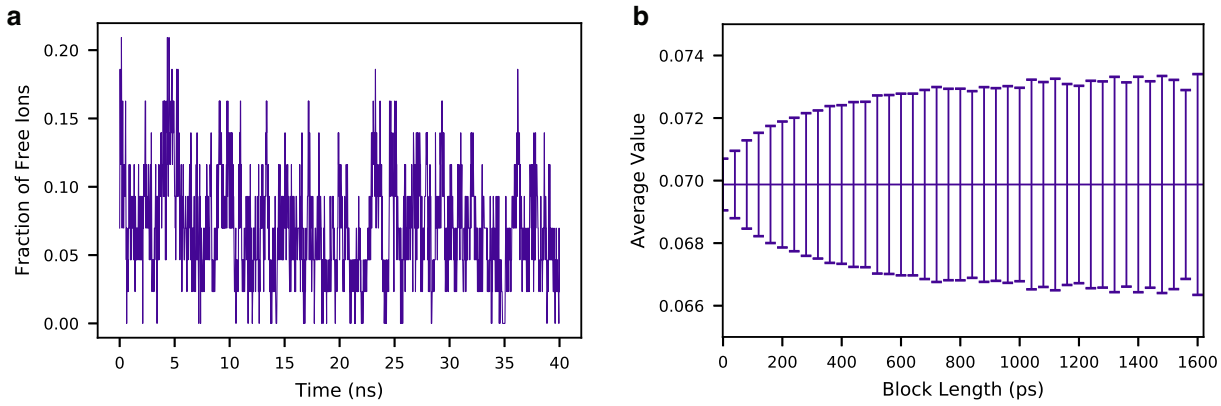

Figure S4: Representative example of block averaging technique. (a) Fraction of free lithium ions as an example of a system property which fluctuates over time. (b) Average value with standard deviation as a function of block length.

Table S1: Details on simulation setup at each concentration.

Li^+ Concentration (mol/L)	Number of Solvent Molecules	Simulation Box Length (Å)
0.05	12108	112.87
0.10	6054	89.81
0.19	3027	71.70
0.47	1211	53.87
0.85	605	43.88
0.98	505	41.82

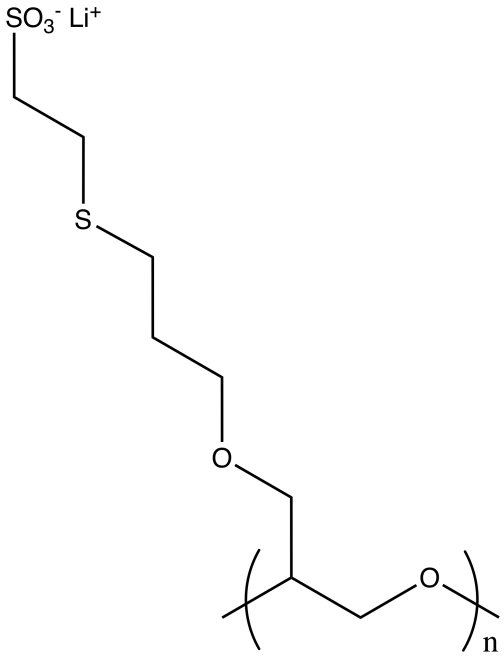

Figure S5: Structure of the PAGELS polyelectrolyte. In this work, $n = 43$.

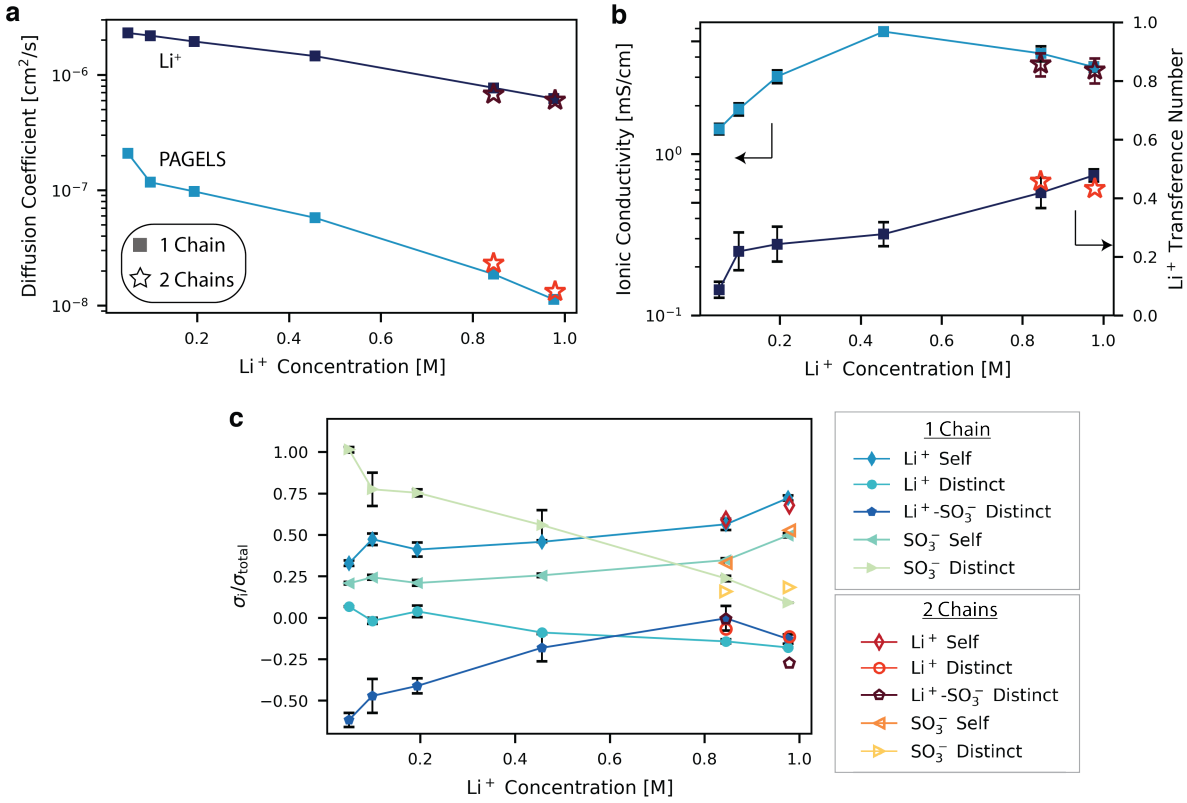

Figure S6: Transport data for simulations using one polymer chain (identical to the data shown in the main text) and using two chains at the two highest concentrations studied. (a) Diffusion coefficients. (b) Ionic conductivity and transference number. (c) Fractional contributions of each type of uncorrelated (self) or correlated (distinct) ion motion to the total conductivity.

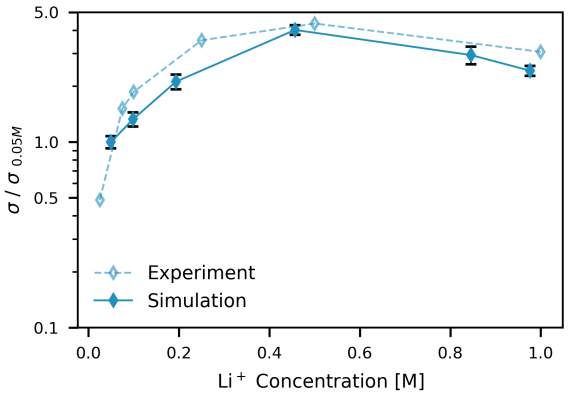

Figure S7: Experimental and computed ionic conductivity normalized by the conductivity at 0.05 M. Overlap of the two curves demonstrates that the simulations have adequately captured the trend in conductivity.

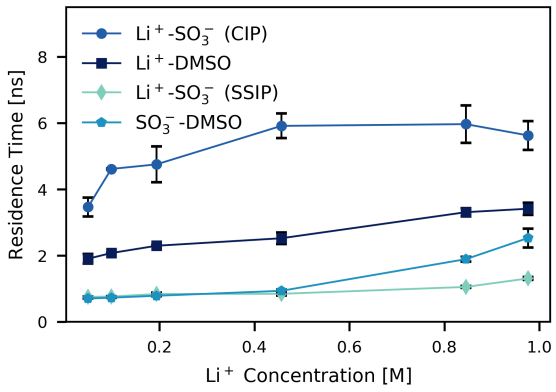

Figure S8: Residence time (characteristic time travelled together by a pair of neighboring species before separating) as a function of concentration for various species.

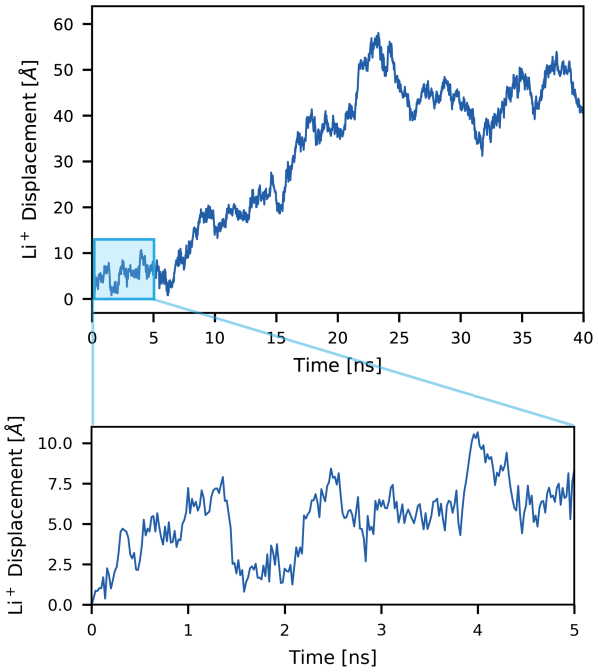

Figure S9: Full 40 ns trajectory of the representative lithium ion shown in Figure 4b of the main text. The zoomed-in portion of the trajectory is identical to that of Figure 4b.

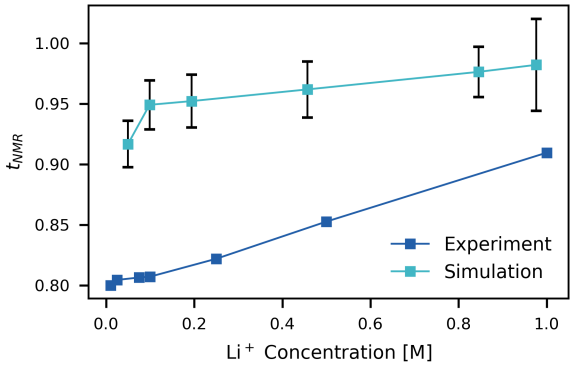

Figure S10: Transport number (t_{NMR}) calculated from both experimental and simulated diffusion coefficients using Eq. (5) of the main text with $z_- = -1$. Experimental data are taken from Buss et al.[S20]

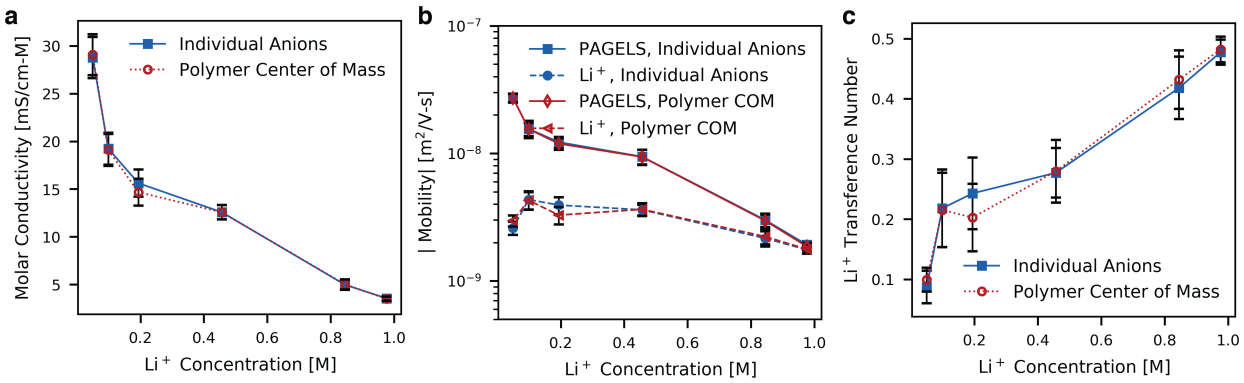

Figure S11: Demonstration that ionic conductivity trends can be equivalently analyzed considering the motion of individual anions or the polymer center of mass. (a) Molar conductivity, (b) electrophoretic mobility, and (c) cation transference number obtained through both of these analysis methods.

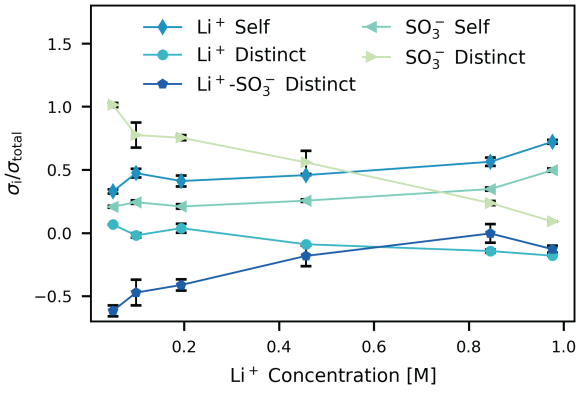

Figure S12: Fractional contributions of each type of uncorrelated (self) or correlated (distinct) ion motion to the total conductivity.

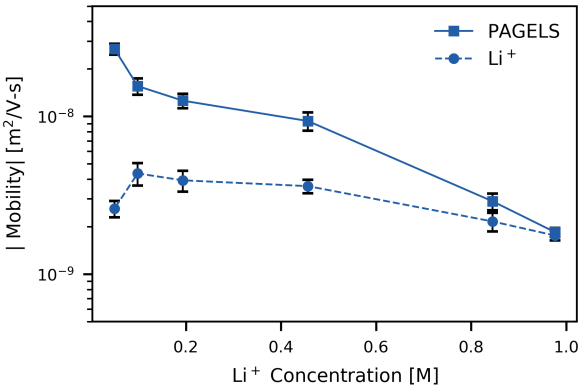

Figure S13: Electrophoretic mobility of the PAGELS polymer and lithium ion as a function of concentration. The absolute value of the data is shown, as the anionic polymer mobility is negative.

References

(S1) Hagberg, A. A.; Schult, D. A.; Swart, P. J. Exploring network structure, dynamics, and function using NetworkX. Proceedings of the 7th Python in Science Conference. Pasadena, CA, 2008; pp 11–15.

(S2) Shannon, P.; Markiel, A.; Ozier, O.; Baliga, N. S.; Wang, J. T.; Ramage, D.; Amin, N.; Schwikowski, B.; Ideker, T. Cytoscape: a software environment for integrated models of biomolecular interaction networks. *Genome research* **2003**, *13*, 2498–504.

(S3) Kaburagi, M.; Yamada, H.; Miyakawa, T.; Morikawa, R.; Takasu, M.; Kato, T. A.; Uesaka, M. Molecular dynamics simulation of telomeric single-stranded DNA and POT1. *Polymer Journal* **2016**, *48*, 189–195.

(S4) Ha, B. Y.; Thirumalai, D. Electrostatic persistence length of a polyelectrolyte chain. *Macromolecules* **1995**, *28*, 577–581.

(S5) Ullner, M.; Woodward, C. E. Orientational correlation function and persistence lengths of flexible polyelectrolytes. *Macromolecules* **2002**, *35*, 1437–1445.

(S6) Carrillo, J.-M. Y.; Dobrynin, A. V. Polyelectrolytes in salt solutions: Molecular dynamics simulations. *Macromolecules* **2011**, *44*, 5798–5816.

(S7) Gubarev, A.; Carrillo, J.-M. Y.; Dobrynin, A. V. Scale-dependent electrostatic stiffening in biopolymers. *Macromolecules* **2009**, *42*, 5851–5860.

(S8) Bačová, P.; Košovan, P.; Uhlík, F.; Kuldová, J.; Limpouchová, Z.; Procházka, K. Double-exponential decay of orientational correlations in semiflexible polyelectrolytes. *The European Physical Journal E* **2012**, *35*, 53.

(S9) Manghi, M.; Netz, R. R. Variational theory for a single polyelectrolyte chain revisited. *The European Physical Journal E* **2004**, *14*, 67–77.

(S10) Kowsari, M. H.; Alavi, S.; Najafi, B.; Gholizadeh, K.; Dehghanpisheh, E.; Ranjbar, F. Molecular dynamics simulations of the structure and transport properties of tetrabutylphosphonium amino acid ionic liquids. *Physical Chemistry Chemical Physics* **2011**, *13*, 8826.

(S11) Hall, L. M.; Stevens, M. J.; Frischknecht, A. L. Dynamics of model ionomer melts of various architectures. *Macromolecules* **2012**, *45*, 8097–8108.

(S12) Liu, H.; Maginn, E. A molecular dynamics investigation of the structural and dynamic properties of the ionic liquid 1-n-butyl-3-methylimidazolium bis(trifluoromethanesulfonyl) imide. *Journal of Chemical Physics* **2011**, *135*, 124507.

(S13) Frenkel, D.; Smit, B. *Understanding molecular simulation: From algorithms to applications*, 2nd ed.; Academic Press, 2001; Vol. 50.

(S14) Solano, C. J.; Jeremias, S.; Paillard, E.; Beljonne, D.; Lazzaroni, R. A joint theoretical/experimental study of the structure, dynamics, and Li^+ transport in bis([tri]fluoro[methane]sulfonyl)imide [T]FSI-based ionic liquids. *Journal of Chemical Physics* **2013**, *139*, 034502.

(S15) Borodin, O.; Smith, G. D.; Henderson, W. Li^+ cation environment, transport, and mechanical properties of the LiTFSI doped N-methyl-N-alkylpyrrolidinium$^+$TFSI$^-$ ionic liquids. *Journal of Physical Chemistry B* **2006**, *110*, 16879–16886.

(S16) Rumble, C. A.; Uitvlugt, C.; Conway, B.; Maroncelli, M. Solute rotation in ionic liquids: size, shape, and electrostatic effects. *The Journal of Physical Chemistry B* **2017**, *121*, 5094–5109.

(S17) Kremer, F., Schönhals, A., Eds. *Broadband Dielectric Spectroscopy*; Springer Berlin Heidelberg: Berlin, Heidelberg, 2011.

(S18) Flyvbjerg, H.; Petersen, H. G. Error estimates on averages of correlated data. *The Journal of Chemical Physics* **1989**, *91*, 461–466.

(S19) Grossfield, A.; Zuckerman, D. M. Quantifying uncertainty and sampling quality in biomolecular simulations. *Annual reports in computational chemistry* **2009**, *5*, 23–48.

(S20) Buss, H. G.; Chan, S. Y.; Lynd, N. A.; McCloskey, B. D. Nonaqueous polyelectrolyte solutions as liquid electrolytes with high lithium ion transference number and conductivity. *ACS Energy Letters* **2017**, *2*, 481–487.